ORIGINAL

Vibrio parahaemolyticus induces inflammation-associated fluid accumulation via activation of the cystic fibrosis transmembrane conductance regulator

Hitomi Iba[1, 2], Takaaki Shimohata[1], Junko Kido[1], Sho Hatayama[1], Takashi Uebanso[1], Kazuaki Mawatari[1], and Akira Takahashi[1]

[1]*Department of Preventive Environment and Nutrition, Institute of Biomedical Sciences, Tokushima University, Tokushima Japan,* [2]*Department of Health and Nutrition, Nagasaki International University Nagasaki Japan*

Abstract : *Vibrio parahaemolyticus* is a foodborne bacterium that causes acute gastroenteritis through the consumption of contaminated, raw, or undercooked seafood. Cystic fibrosis transmembrane conductance regulator (CFTR) is a well-characterized chloride channel that regulates several other ion channels and transporters to maintain water homeostasis in the gut lumen. Also, CFTR is a main target of bacterial infection-associated diarrhea. Hence, the aim of this study was to clarify the contribution of CFTR in *V. parahaemolyticus*-induced diarrhea in a mouse model of intestinal loop fluid accumulation, with CFTR inhibitors and a CFTR knockout model. The results indicated that CFTR plays a critical role in fluid accumulation in response to *V. parahaemolyticus* infection. We also investigated the inflammatory association in CFTR-mediated *V. parahaemolyticus*-induced fluid secretion with cyclooxygenase inhibitors and found that fluid accumulation was decreased by inhibition of cyclooxygenase 2 produced by neutrophils. These findings suggest that *V. parahaemolyticus*-inducing infiltration and activation of neutrophils also participated in CFTR mediated fluid secretion. This study reveals an important relationship between *V. parahaemolyticus*-induced diarrhea and inflammation in a mouse model. J. Med. Invest. 68 : 59-70, February, 2021

Keywords **:** *CFTR, COX-2, diarrhea, inflammation, Vibrio parahaemolyticus*

INTRODUCTION

Vibrio parahaemolyticus is a marine, halophilic, Gram-negative bacterium that causes acute gastroenteritis via the consumption of contaminated, raw, or undercooked seafood with clinical symptoms manifesting as diarrhea, abdominal cramps, nausea, vomiting, and fever (1). Moreover, biopsies indicate that *V. parahaemolyticus* infection causes a disruption to the intestinal epithelium along with inflammation (2), suggesting that the clinical symptoms are largely associated with inflammation. The signs of *V. parahaemolyticus* infection have been observed by the intestinal loop test of rabbit ileal and an oral inoculation model of infant rabbits (3, 4).

For many years, thermostable direct hemolysin (TDH) and TDH-related hemolysin (TRH) have been considered as the main pathogenicity factors of *V. parahaemolyticus*. TDH forms pore complexes in the host cell membrane, resulting in hemolysis and cytotoxicity (5-8). TDH allows the flow of both water and ions across the host membrane, which induces Cl- secretion (9, 10). TRH is immunologically related to TDH and induces Cl- secretion similar to the TDH (11). In fact, a TDH-deficient mutant decreased fluid accumulation but which strain showed partial fluid accumulation in a rabbit model (12). On the other hand, strains lacking the type 3 secretion system (T3SS) 2, which is encoded on chromosome 2 (T3SS2), failed to induce diarrhea and infection-associated inflammation in these animal models (3, 13). Reportedly, the mechanism of T3SS2 mediated diarrhea was revealed in detail that induced by VopV effector, an F-actin-binding protein, and TDH secreted by T3SS2 system (14, 15). These data strongly suggest that the TDH and T3SS2 are the main virulence factor in *V. parahaemolyticus*-induced diarrhea (3, 4, 16, 17).

In contrast to the T3SS2, T3SS1, a second secretion system that is encoded on chromosome 1, is found in all *V. parahaemolyticus* strains including nonpathogenic isolates (18). The virulence of the T3SS1 has been associated with cytotoxicity and cytokine production in cultured cell models (3, 5, 19-22). Despite the strong virulence observed in *in vitro* studies, the T3SS1 plays only a relatively minor role in pathogenesis within the animal gastrointestinal tract (3, 4). Thus, the contribution of the T3SS1 to the clinical symptoms of *V. parahaemolyticus* infection, particularly diarrhea and inflammation, remains unclear.

The mucosal layer of the intestinal tract acts as a defense system against infection by preventing attachment and accumulation of pathogenic bacteria. Accordingly, several ion channels and transporters closely maintain cellular homeostasis in the mucosal layer. During the infection process, several ion channels and transporters are excessively activated by virulence factors, which lead to failed ion homeostasis and the onset of diarrhea via disruption of the balance of electrolyte absorption and secretion (23). Severe diarrhea causes loss of body water and electrolytes, which lead to dehydration and acidosis. Notably, diarrhea can be especially fatal to infants, the elderly, and the disabled.

It is known that infection of pathogenic bacteria, such as *Vibrio cholerae*, enterotoxigenic *Escherichia coli* (ETEC), and enteropathogenic *E. coli*, causes excessive fluid loss, which leads to secretory diarrhea. The mechanisms of secretory diarrhea caused by infection with *V. cholerae* and ETEC have been described in previous reports. Cholera toxin and heat-stable enterotoxin produced by ETEC activate the cystic fibrosis transmembrane conductance regulator (CFTR), which leads to the production of

Received for publication October 5, 2020 ; accepted October 30, 2020.

Address correspondence and reprint requests to Takaaki Shimohata, Department of Preventive Environment and Nutrition, Institute of Biomedical Sciences, Tokushima University, 2 Chome-24 Shinkuracho, Tokushima, 770-8501, Japan and Fax : +81-88-633-7092.

cyclic adenosine monophosphate (cAMP) and cyclic guanosine monophosphate (24, 25). Moreover, overactivation of CFTR causes increased secretion of anions and fluid, which leads to severe diarrhea.

Although CFTR plays a key role in secretory diarrhea, its contribution to *V. parahaemolyticus*-induced severe diarrhea remains unclear, as few studies have examined the association between CFTR activity and TDH or TRH with a focus on toxin secretion (11). Therefore, the aim of the present study was to determine the contribution of CFTR in *V. parahaemolyticus*-induced severe diarrhea with the use of living bacteria and an in vivo mouse model of intestinal infection. A secondary aim was to assess the extent of inflammation associated with CFTR-mediated fluid imbalance caused by *V. parahaemolyticus* infection. The results of this study demonstrate that the production of prostaglandin E2 (PGE2) via cyclooxygenase 2 (COX-2) produced by neutrophils activated CFTR and induced diarrhea. These data strongly suggest that *V. parahaemolyticus*-induced inflammation also participates in the induction of diarrhea. In addition, the efficacy of diarrhea treatment targeting *V. parahaemolyticus*-induced inflammation was investigated.

MATERIALS AND METHODS

Bacterial strains and culture conditions

V. parahaemolyticus strain RIMD2210633 (Kanagawa phenomenon-positive, serotype O3 : K6) was used as a standard strain. The bacteria were cultured at 37℃ with shaking in Luria–Bertani medium supplemented with 3% NaCl. Deletion mutant strains (DtdhAS, DT3SS1, DT3SS2) were previously described (3, 12, 26).

Preparation of bacterial suspension

V. parahaemolyticus cells were collected after overnight culture by centrifugation and washed two times in phosphate-buffered saline (PBS). The optical density of the bacterial suspension was adjusted to 1.0 at a wavelength of 600 nm (OD_{600}) with PBS.

Animals

6-week-old C57BL/6J male mice (Japan SLC, Tokyo, Japan or Charles River Japan, Kanagawa, Japan) were obtained from Japan SLC (Tokyo, Japan) and Charles River Japan (Kanagawa, Japan). After 1-week adaption, that mice were used for infection experiment. The *Cftr*$^{tm1Unc+/-}$ mouse were originally obtained from The Jackson Laboratory (Bar Harbor ME, USA.), that mouse was bred onto the C57BL/6J background until congenic. *Cftr*$^{tm1Unc+/-}$ mice were bread to obtain *Cftr*$^{tm1Unc-/-}$ (*CFTR*$^{-/-}$: CFTR knockout mice) and *Cftr*$^{tm1Unc+/+}$ (*CFTR*$^{+/+}$: WT) mice. WT and CFTR knockout mice were fed a liquid diet (ENSURE LIQUD : ABBOTT JAPAN, Tokyo) to prevent the lethal intestinal obstruction in CFTR knockout mice. 7-week-old WT and CFTR knockout male mice were used for loop assay.

Mouse intestinal loop assay

WT C57BL/6J mice and CFTR knockout mouse were used for the mouse intestinal loop assay (27, 28). About creation of loops, mice were anesthetized, and small abdominal incision was made to expose the intestine. During the surgery, body temperature was maintained at 38°C using a heating pad. For the jejunal closed-loop model, 2–3-cm loops were created by sutures. *V. parahaemolyticus* bacterial suspension (250 μL, OD_{600} = 1.0) prepared in PBS or just PBS alone (250 μL) was injected into the intestinal loops and infection was allowed for 4 h. Loop assay was applied one loop in one mouse for each condition. After infection, the intestinal loops were removed, and fluid accumulation was quantified by determining the loop weight/length ratio. To investigate the role of CFTR in diarrhea, glybenclamide (final concentration, 300 μM ; Sigma-Aldrich Corporation, St. Louis, MO, USA), 2-(phenylamino) benzoic acid (DPC ; 500 μM ; Wako Pure Chemical Industries, Ltd., Osaka, Japan), and a CFTR inhibitor were individually added to the *V. parahaemolyticus* bacterial suspension (OD_{600} = 1.0). Furthermore, to examine the relationship between COX and diarrhea, indomethacin (5 mg/kg ; Sigma-Aldrich Corporation) and NS398 (5 mg/kg ; Sigma-Aldrich Corporation) were individually added to the *V. parahaemolyticus* bacterial suspension (OD_{600} = 1.0), which was then injected into the intestinal loops.

Cell culture

RAW264.7 cells were cultured in Dulbecco's Modified Eagle's Medium (DMEM ; Sigma-Aldrich Corporation) supplemented with 10% fetal bovine serum (FBS ; Gibco BRL) and 100 μg/mL gentamicin (Sigma-Aldrich Corporation). The cells were seeded on 6-well culture dashers at a density of 1×10^6 cells/well. RAW264.7 cells that had been cultured for 4 days were used for subsequent experiment.

Isolation of intraperitoneal macrophages

In order to isolate the intraperitoneal macrophages, 7-week-old C57BL/6J mice were infected with 2 ml thioglycolate medium intraperitoneally. After 4 days, mice were euthanized, and macrophages were collected with ice-cold PBS. The cells were centrifuged at 1,000 rpm for 10 min at 4℃ and resuspended with RPMI1640 medium (GIBCO BRL). After washing with RPMI1640, the cells were resuspended with RPMI1640 medium containing with 10% FBS and 100 μg/mL gentamicin and seeded on 24-well culture dashers at a density of 1×10^6 cells/ well.

Infection protocol of in vitro experiment

At least, 1 hours before infection, the culture medium of RAW264.7 cells and isolated intraperitoneal macrophages were replaced with fresh DMEM (without supplements) or RPMI1640 (without supplements), respectively. After cultivation, bacteria were washed and resuspended in PBS. Bacteria were added to each well (1×10^7 colony-forming units/dish).Infection were allowed to proceed at 37℃ in 5% CO_2.

Analysis by capillary electrophoresis-time of flight mass spectrometry (CE-TOFMS)

Briefly, 30 mg of frozen mouse intestinal samples were transferred into 500 μL of methanol containing an external standard (50 μM) and homogenized with zirconia beads using a Multi-beads shocker®. To remove the phospholipid content, 500 μL of chloroform and 200 μL of Milli-Q water were added to the homogenate, which was then vortexed for 30 s and centrifuged at 2,300 × g for 5 min at 4℃. The aqueous layer was prepared by centrifugal ultrafiltration at 9,100 × g and 4℃ to remove proteins and completely dried in a vacuum centrifuge. Then, the dried samples were dissolved in 25 μL of Milli-Q water to prepare the metabolites. The samples were analyzed using a CE-TOFMS system (Agilent Technologies, Santa Clara, CA, USA).

HE staining

Mouse intestinal loops were washed with PBS and fixed in 4% paraformaldehyde for 2 days, then embedded in paraffin and sliced into 3 μm-thick sections, which were plated on glass slides. The slides were stained with HE, mounted in malinol (Muto Pure Chemicals, Co., Ltd., Tokyo, Japan), and observed under an OLYMPUS BX50 microscope (Olympus Corporation, Tokyo, Japan).

Western blot analysis

Mouse intestinal loops were removed after infection, cut open, and washed with PBS. The epithelial tissues of the loops were placed in radioimmunoprecipitation assay buffer (500 μL) and homogenized. After centrifugation, the supernatant was collected. Proteins (50 μg) were resolved by 8% sodium dodecyl sulfate-polyacrylamide gel electrophoresis and transferred to polyvinylidene difluoride membranes. The membranes were blocked for 60 min in 3% skim milk in Tris-buffered saline with Tween 20 (TBST) and washed three times with TBST for 10 min. Then, the membranes were incubated overnight with a primary rabbit anti-COX-1 antibody (Ab) (dilution, 1 : 1000 ; Cayman Chemical Company, Ann Arbor, MI, USA), mouse anti-COX-2 Ab (1 : 1000 ; BD Biosciences, San Jose, CA, USA), rabbit anti-myeloperoxidase (MPO) heavy chain Ab (1 : 1000 ; Santa Cruz Biotechnology, Inc., Dallas, TX, USA), and rabbit anti-β actin Ab (1 : 1000 ; Santa Cruz Biotechnology, Inc.) diluted in 3% skim milk in TBST. The membranes were washed three times with TBST for 10 min and incubated for 2 h with a secondary Ab : anti-rabbit immunoglobulin (Ig)G (1 : 2000 ; BioSource International, Inc., San Diego, CA, USA) or anti-mouse IgG (1 : 2000 ; BioSource International, Inc.) diluted in 3% skim milk in TBST. After washing, bound Abs were detected using enhanced chemiluminescence reagent (Tris, 100 mM ; luminol, 1.25 mM ; p-coumaric acid, 225 μM ; pH 8.5). Bands were scanned in a luminescent image analyzer (LAS-3000 UV mini ; Fujifilm Global, Tokyo, Japan).

RNA extraction and reverse transcription

Mouse intestinal loops were removed after infection, cut open, and washed with PBS. Total RNA from the epithelial tissues of the loops was extracted using TRIzol reagent (Thermo Fisher Scientific, Waltham, MA, USA). The RNA was treated with RNase-free DNase I (Takara Bio, Inc., Shiga, Japan) to eliminate contaminating DNA. Reverse transcription of RNA (1.0 μg) was performed using the PrimeScript RT-Reagent Kit (Takara Bio, Inc.).

Real-time reverse transcription-polymerase chain reaction. (Real-time RT-PCR)

Real-time RT-PCR was performed using 2 μL of reverse-transcribed product, 0.2 μM of each primer, and 10 μL of SYBR Premix Ex *Taq* polymerase (Takara Bio, Inc.) with a LightCycler Real-Time PCR System (Roche, Basel, Switzerland) and specific primers listed in Table 1. 18S ribosomal RNA was used as an internal standard to normalize mRNA expression levels of COX-1, COX-2, IL-1β, MIP-2, MCP-1 and TNF-α.

Immunostaining

The loops were embedded in paraffin as described above. After deparaffinization, the tissue sections were blocked for 60 min in 1% bovine serum albumin (BSA) in PBS, then incubated overnight with a primary Ab (rabbit anti-COX-2, 1 : 250, BD Biosciences) diluted in 1% BSA solution at 4℃. Afterward, the tissues were washed with PBS prior to incubation with a secondary Ab (Alexa fluor488, 1 : 250, Thermo Fisher Scientific) in 1% BSA solution for 60 min in the dark and then washed with PBS again. In addition, the slides were incubated overnight with primary Ab (rabbit anti-MPO heavy chain, 1 : 500, Santa Cruz Biotechnology, Inc.) in 1% BSA solution at 4℃, then washed with PBS and incubated with a secondary Ab (Alexa fluor568, 1 : 250, Thermo Fisher Scientific) in 1% BSA solution at room temperature for 60 min. After washing with PBS, the slides were incubated with 4′, 6-diamidino-2-phenylindole dihydrochloride (143 nM ; Thermo Fisher Scientific) in PBS for 5 min at room temperature. Afterward, the slides were washed with PBS and mounted with Fluorescent Mounting Medium (Dako, Glostrup, Denmark). Fluorescent images of the slides were obtained with an OLYMPUS BX50 microscope (Olympus Corporation).

Statistical analysis

Statistical analysis was performed using the Student's *t*-test or one-way analysis of variance (ANOVA) with Tukey kramer's test with Statcel 4. (OMS Publishing, Tokorozawa, Japan). A probability (*p*) value of > 0.05 or 0.01 were considered statistically significant.

RESULTS

Contribution of CFTR in V. parahaemolyticus-induced fluid accumulation as determined with the mouse intestinal loop test

To evaluate the relationship between CFTR and fluid accumulation in *V. parahaemolyticus* infection, the mouse intestinal loop assay was performed with the use of CFTR inhibitors. The results of the mouse intestinal loop assay showed that infection with *V. parahaemolyticus* for 4h increased fluid accumulation (AV ± SD : 0.090 ± 0.033) as compared with non-infected loops (0.050 ± 0.009) (Fig 1A). Glybenclamide and DPC (a CFTR inhibitor) treatment attenuated fluid accumulation in *V. parahaemolyticus*-infected mouse loops (VP + Glybenclamide ; 0.070 ± 0.019, VP + DPC ; 0.049 ± 0.009), to levels similar to that of non-infected loops (0.050 ± 0.009). We have confirmed that this inhibitor does not affect the viability of the bacteria (Fig S1). Next, CFTR knockout mice were used to elucidate the contribution of CFTR in *V. parahaemolyticus*-induced fluid accumulation. As shown in Fig 1B, *V. parahaemolyticus* infection failed to induce fluid accumulation in the CFTR knockout mice (0.061 ± 0.019). These data indicate that *V. parahaemolyticus* induced CFTR-mediated fluid accumulation in the mouse loop model.

V. parahaemolyticus infection induced elevation of PGE2 and γ-aminobutyric acid (GABA)

CE-TOFMS metabolome analysis was performed to elucidate the effect of CFTR activation during *V. parahaemolyticus* infection

Table 1. Sequences of the primers used for Real-time RT-PCR.

	primer sequence (5'-3')	
gene	forward	reverse
COX-1	ACTATCCGTGCCAGAACCAG	AGAGAATTCCGAAGCCAGGT
COX-2	TGGTGAAACTCTGGACAGAC	GGGTAGATCATCTCTACCTG
18S	AAACGGCTACCACATCCAAG	GGCCTCGAAAGAGTCCTGTA
IL-1β	GACCTTCCAGGATGAGGACA	TAATGGGAACGTCACACACC
MIP-2	GCCAAGGGTTGACTTCAAGA	CTTCAGGGTCAAGGGAAACT
MCP-1	CCCAATGAGTAGGCTGGAGA	TCTGGACCCATTCCTTCTTG
TNF-α	ATGGCCTCCCTCTCATCAGTT	ACAGGCTTGTCACTCGAATTTTG

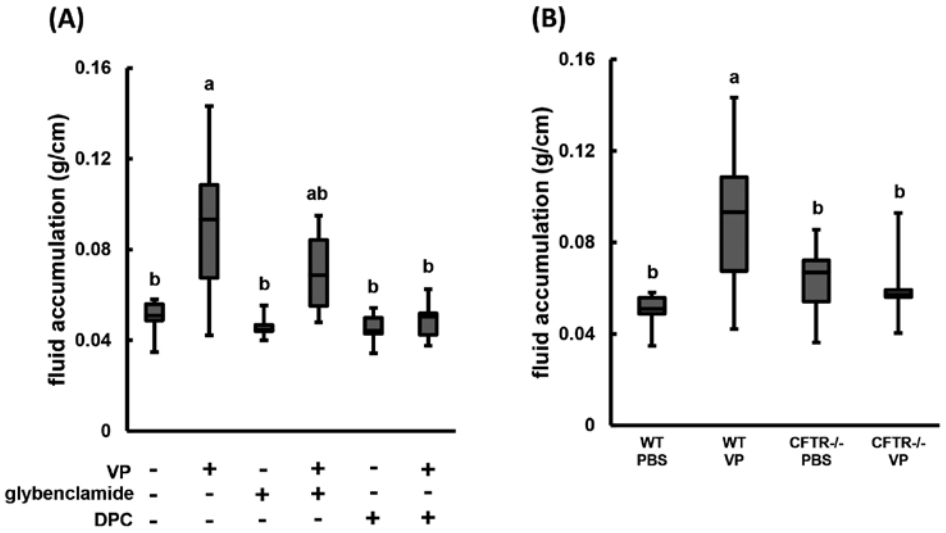

Fig 1. CFTR association with *V. parahaemolyticus*-induced fluid accumulation. (A) Bacterial suspensions with CFTR inhibitors were injected into mouse intestinal loops. After infection for 4 h, the loops were removed and fluid accumulation was calculated (n = 5 to 8). Upper horizontal line of box, 75th percentile ; lower horizontal line of box, 25th percentile ; horizontal bar within box, median ; upper horizontal bar outside of box, maximum value ; lower horizontal bar outside of box, minimum value. Different letters of the alphabet indicate statistical difference ($p < 0.05$) from each other as determined by ANOVA with Tukey Kramer's test. (B) Bacterial suspension or PBS was injected to the intestinal loops of CFTR knockout mouse. After infection for 4 h, the loops were removed and fluid accumulation was calculated (n = 5 to 7). Box plot showing fluid accumulation, as determined with a mouse intestinal loop assay. Upper horizontal line of box, 75th percentile ; lower horizontal line of box, 25th percentile ; horizontal bar within box, median ; upper horizontal bar outside of box, maximum value ; lower horizontal bar outside of box, minimum value. Different letters of the alphabet indicate statistical difference ($p < 0.05$) from each other as determined by ANOVA with Tukey Kramer's test.

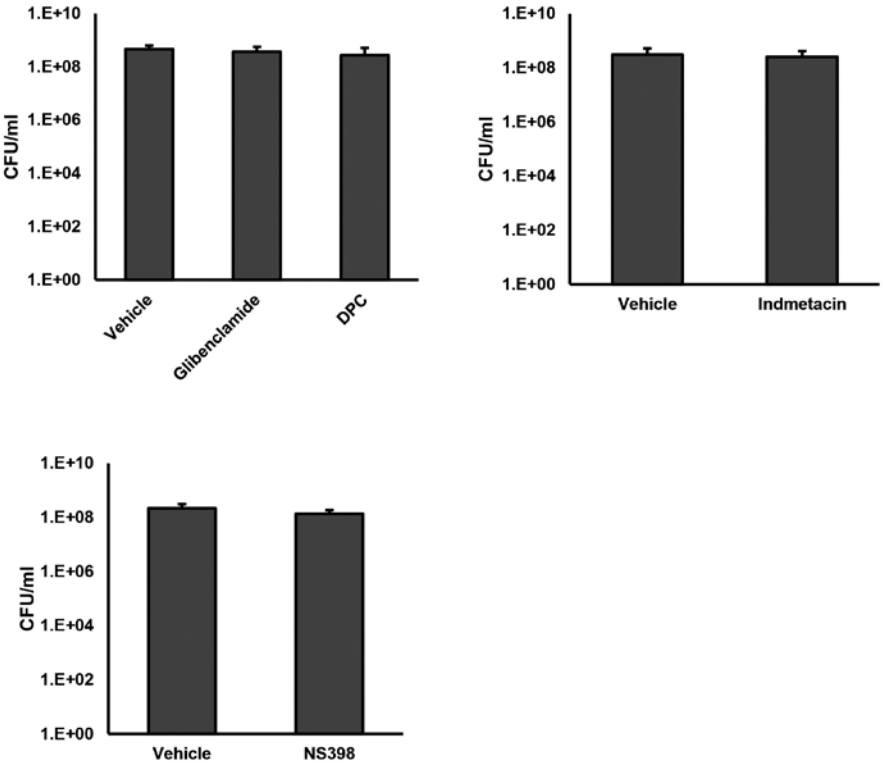

Fig S1. Effect of each inhibitors on bacterial viability. The bacterial cells were incubated with each inhibitors at 37℃ for 6 h. After that, the cells were separated on LB agar plate and incubated at 37℃ for 16 h. The bacterial viability was estimated with colony number. Those data indicated that each inhibitor did not affect bacterial viability. The error bar indicates standard deviation.

for 4 h of mouse ileal tissue (Fig S2). Because the infection process was relatively short term, there was no significant difference between the infected and non-infected samples. However, there were some differences in CFTR activity-associated components. Specifically, *V. parahaemolyticus* infection increased PGE2 production by 1.4-fold ($p = 0.045$) and GABA production by 1.8-fold ($p = 0.003$) in the mouse intestinal loops (Fig S3).

COX-2 inhibitor decreased fluid accumulation in the mouse intestine

Intracellular cAMP production is regulated by PGE2, which in turn is regulated by COX catalysis. So, we next investigated the contribution of COX-mediated PGE2 production to the accumulation of fluid in the mouse intestinal loop with the use of three different types of COX inhibitors and found that treatment with indomethacin (a COX inhibitor) (0.051 ± 0.017) and NS398 (a selective COX-2 inhibitor) (0.062 ± 0.011) attenuated *V. parahaemolyticus*-induced fluid accumulation (Fig 2). Those inhibitors did not affect the viability of the bacteria (Fig S1). These data strongly suggest that COX-2-mediated PGE2 production participates in *V. parahaemolyticus*-induced fluid accumulation in the mouse intestine.

COX-2 expression was up-regulated in V. parahaemolyticus

In order to identify the PGE2-producing cells, histological changes to *V. parahaemolyticus*-infected tissue were investigated (Fig 3A-B). After infection with *V. parahaemolyticus*, which revealed inflammation was confirmed by expression of mRNA level in inflammatory cytokine (Fig 3C) and the migration of neutrophils via western blot analysis with the use of Abs against MPO, an established marker of neutrophils (Fig 3D).

Next, western blot and RT-PCR analyses were performed to evaluate COX-2 expression levels in *V. parahaemolyticus*-infected mouse tissue. As shown in Fig 4, COX-1 and COX-2 protein expression level were up-regulated in *V. parahaemolyticus*-infected tissues, but COX-2 was more significantly increased. Further, the mRNA expression levels of COX-1 and COX-2 were analyzed by real-time RT-PCR. Similar to the protein level, COX-2 mRNA expression was increased by *V. parahaemolyticus* infection (Fig 4C).

COX-2 and MPO were co-localized in mouse intestine following infection with V. parahaemolyticus

Next, we investigated the distribution of COX-2 in *V. parahaemolyticus*-infected tissues by immunostaining with Abs against COX-2 and MPO. As shown in Fig 5, COX-2 was expressed in a portion of the neutrophils that had infiltrated the mouse intestine. Meanwhile, MPO was highly co-localized with COX-2. These data suggest that COX-2-mediated PGE2 production was mainly associated with neutrophils cells in *V. parahaemolyticus* infection.

DISCUSSION

It is known that CFTR is main target of bacterial toxin which induces secretary diarrhea. In this study, we found CFTR mediated fluid accumulation in *V. parahaemolyticus* infection, and its channel activation was closely associated with *V. parahaemolyticus*-induces inflammation. In order to estimate the contribution of each *V. parahaemolyticus* virulence factor on COX-2 expression in leucocyte, we used mouse macrophage cell line RAW264.7 cells and peritoneal macrophage cells for *in vitro* infection model. Each virulence factor deletion-mutant (ΔT3SS1, ΔT3SS2, and ΔTDH) indicated COX-2 expression. Moreover T3SS1 deletion mutant induced high-expression level of COX-2 (Fig S4A). Those data indicated that T3SS1, T3SS2, and TDH were not associated with production of COX-2 in leucocyte. On the other hands, even the killed *V. parahaemolyticus* (heat-killed, UVC-killed, gentamycin treated *V. parahaemolyticus*) induced COX-2 expression (Fig S4A-B). It suggest that, COX-2 expression in macrophage cells were easily activated by bacterial endotoxins, such as LPS. However, those killed bacteria could not induced fluid accumulation and neutrophil migration in mouse loop test (Fig S5). Those results suggest that the both migration and activation of neutrophils are necessary for fluid accumulation in a mouse intestinal model of *V. parahaemolyticus* infection.

Taken together, our data suggest that *V. parahaemolyticus* infection induced migration of neutrophils and PGE2 production to the site of infection in a mouse infection model. Furthermore, PGE2 production might activate CFTR-mediated fluid accumulation. These findings illustrate the importance of the inflammatory response in *V. parahaemolyticus*-induced diarrhea, as the production of inflammatory factors was involved in the CFTR-mediated fluid accumulation in response to *V. parahaemolyticus* infection.

There are several pathways involved in the activation of CFTR. In addition, several compounds are known to elevate the intracellular cAMP content by inhibition of phosphodiesterase (a cAMP-degrading enzyme) and activation of adenylyl cyclase (a cAMP-synthesizing enzyme) (29). PGE2 is a known activator of adenylyl cyclase in the intestinal epithelium, and it causes synthesis of cAMP under the catalytic influence of adenylyl cyclase (30). Therefore, we suspect that increasing PGE2 production by neutrophils will upregulate intracellular cAMP content in intestinal epithelial cells. In addition, cell-to-cell crosstalk may activate CFTR-mediated diarrhea. Finally, the roles of cAMP and PGE2 in *V. parahaemolyticus* infection of mouse intestinal tissues were investigated using an enzyme-linked immunosorbent assay and CE-TOFMS system. Unfortunately, there was no definite increase in PGE2 or cAMP production in *V. parahaemolyticus*-infected mouse intestinal tissues (Fig S3). Thus, the direct effect of PGE2 production by neutrophils on CFTR activation in epithelial cells during *V. parahaemolyticus* infection remains unclear. However, there is a possibility that the production of cAMP or PGE2 was limited and biased toward the mucus layers at the site of infection. In this study, cAMP and PGE2 levels were measured in whole tissues, but the production of the target markers may have been downregulated in the base tissue. Therefore, an alternative strategy is needed to investigate the exact production of PGE2 and cAMP during infection, such as the isolation of the mucus layer. Also, we plan to perform future experiments with a co-culture system to reveal the direct effect of PGE2 on CFTR production by neutrophils on epithelial cells.

A previous study revealed that T3SS1 is closely associated with *V. parahaemolyticus*-induced inflammation. T3SS1 effectively activates inflammation-associated signaling cascades, such as the nuclear factor-κβ and mitogen-activated protein kinase pathways (ERK1/2, p38, and JNK) (19, 21, 31). As confirmation of the contribution of T3SS1 in *V. parahaemolyticus*-induced PGE2 production, we observed a tendency where PGE2 production was increased in mouse intestinal tissues in response to *V. parahaemolyticus* production, and the production level was lower in a T3SS1-deletion mutant. However, the PGE2 production level was not significant. Also, T3SS1 may contribute to the inflammatory response via PGE2 production and may partially participate in the activation of CFTR.

Opposite to T3SS1 effectors, the host inflammatory signaling were suppressed by T3SS2 effecter proteins. VopZ suppressed MAPKs and NF-κB pathway by inhibiting TAK1 activation, and it facilitates intestinal colonization (32). Also, VopA inhibit MAPKs signaling pathway by acetylation of catalytic loop (33). Those effectors may affect COX-2 production in infection site.

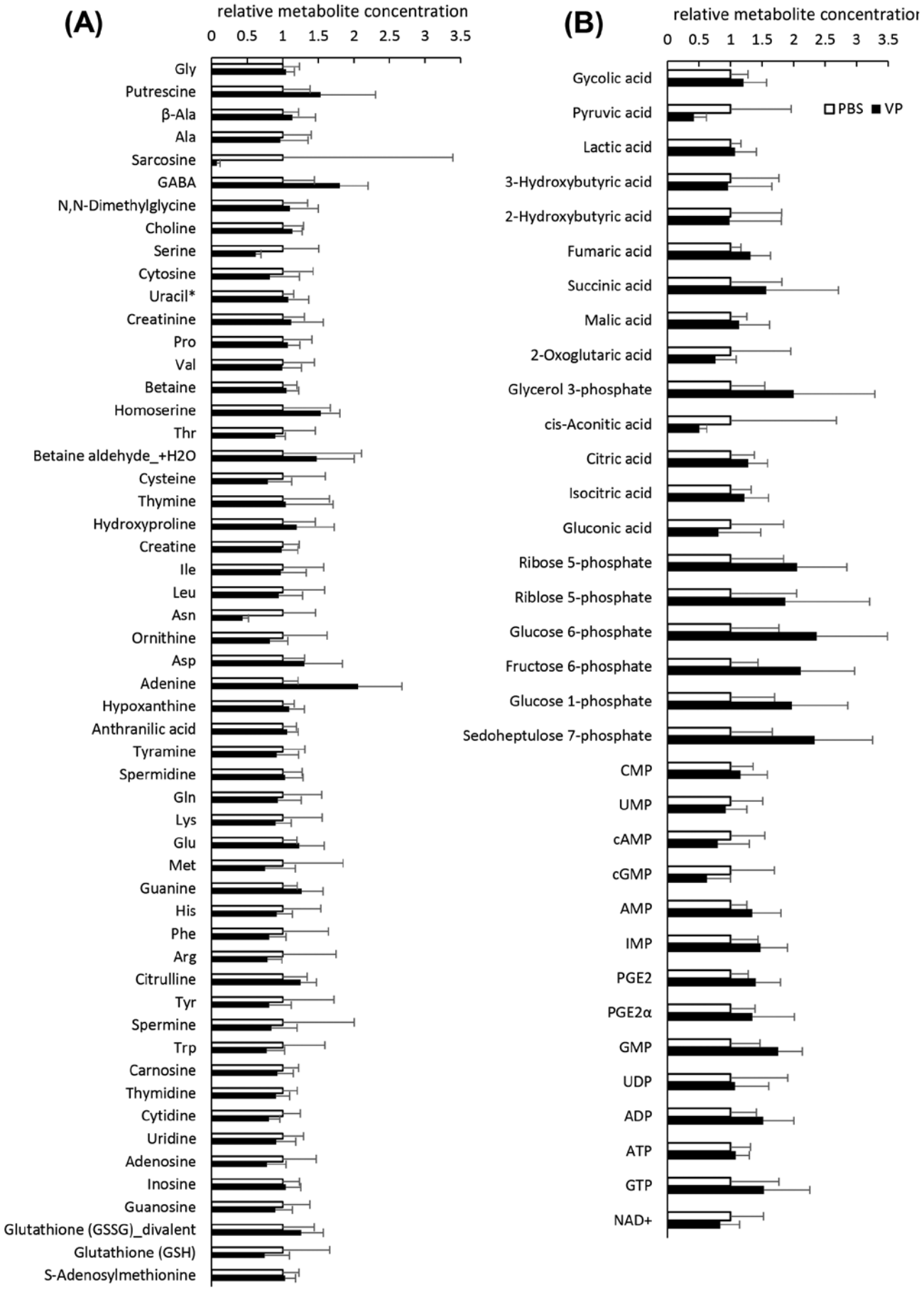
(A)
relative metabolite concentration
0 0.5 1 1.5 2 2.5 3 3.5
Gly
Putrescine
β-Ala
Ala
Sarcosine
GABA
N,N-Dimethylglycine
Choline
Serine
Cytosine
Uracil*
Creatinine
Pro
Val
Betaine
Homoserine
Thr
Betaine aldehyde_+H2O
Cysteine
Thymine
Hydroxyproline
Creatine
Ile
Leu
Asn
Ornithine
Asp
Adenine
Hypoxanthine
Anthranilic acid
Tyramine
Spermidine
Gln
Lys
Glu
Met
Guanine
His
Phe
Arg
Citrulline
Tyr
Spermine
Trp
Carnosine
Thymidine
Cytidine
Uridine
Adenosine
Inosine
Guanosine
Glutathione (GSSG)_divalent
Glutathione (GSH)
S-Adenosylmethionine
(B)
relative metabolite concentration
0 0.5 1 1.5 2 2.5 3 3.5
PBS VP
Gycolic acid
Pyruvic acid
Lactic acid
3-Hydroxybutyric acid
2-Hydroxybutyric acid
Fumaric acid
Succinic acid
Malic acid
2-Oxoglutaric acid
Glycerol 3-phosphate
cis-Aconitic acid
Citric acid
Isocitric acid
Gluconic acid
Ribose 5-phosphate
Riblose 5-phosphate
Glucose 6-phosphate
Fructose 6-phosphate
Glucose 1-phosphate
Sedoheptulose 7-phosphate
CMP
UMP
cAMP
cGMP
AMP
IMP
PGE2
PGE2α
GMP
UDP
ADP
ATP
GTP
NAD+

Fig S2.

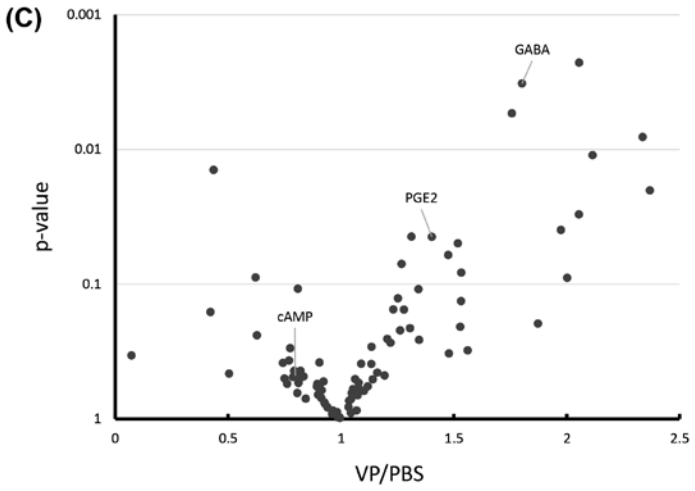

Fig S2. Measure of metabolome in mouse intestinal mucosa infected with *V. parahaemolyticus* analyzed by CE-TOFMS. The amount of metabolites in *V. parahaemolyticus*-infected mouse intestinal mucosa were isolated from loop assay tissue and analyzed by CE-TOFMS. Those data were categorized in cationic metabolites (A) and anionic metabolites (B), respectively. The error bar indicates standard deviation. Data differing significantly from PBS are marked by * (Student's *t*-test) (n = 8). *$p < 0.05$. Relative quantitative comparisons were described (C).

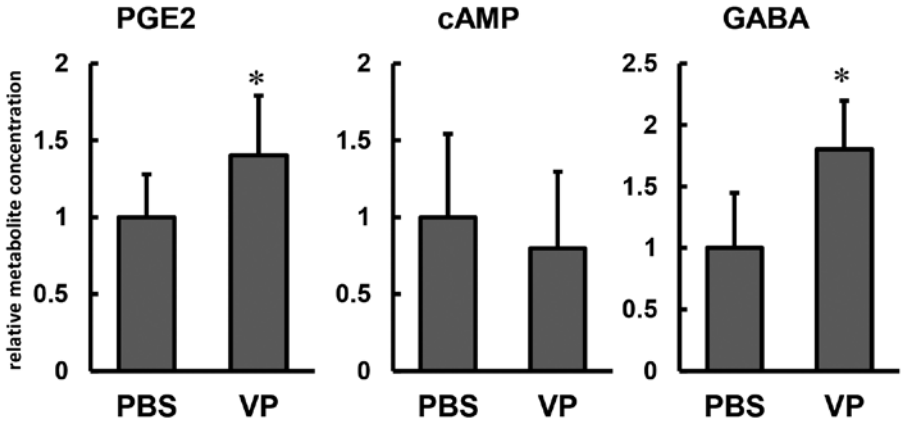

Fig S3. Production of PGE2, cAMP and GABA in mouse intestinal mucosa infected with *V. parahaemolyticus* analyzed by CE-TOFMS. The amount of CFTR activator in *V. parahaemolyticus*-infected mouse intestinal mucosa were isolated from loop assay tissue and estimated by CE-TOFMS. The error bar indicates standard deviation. Data differing significantly from PBS are marked by * (Student's *t*-test) (n = 8). *$p < 0.05$.

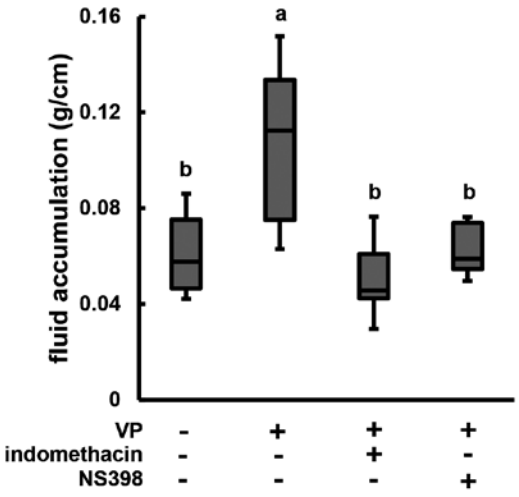

Fig 2. COX contribution to *V. parahaemolyticus*-induced fluid accumulation. Bacterial suspensions with COX inhibitors (indomethacin or NS398) were injected to mouse intestinal loops. After infection for 4 h, fluid accumulation was calculated (n = 6 to 8). Box plot showing fluid accumulation, as determined by the mouse intestinal loop assay with COX inhibitors. Upper horizontal line of box, 75th percentile ; lower horizontal line of box, 25th percentile ; horizontal bar within box, median ; upper horizontal bar outside of box, maximum value ; lower horizontal bar outside of box, minimum value. Different letters of the alphabet indicate statistical difference ($p < 0.01$) from each other as determined by ANOVA with Tukey Kramer's test.

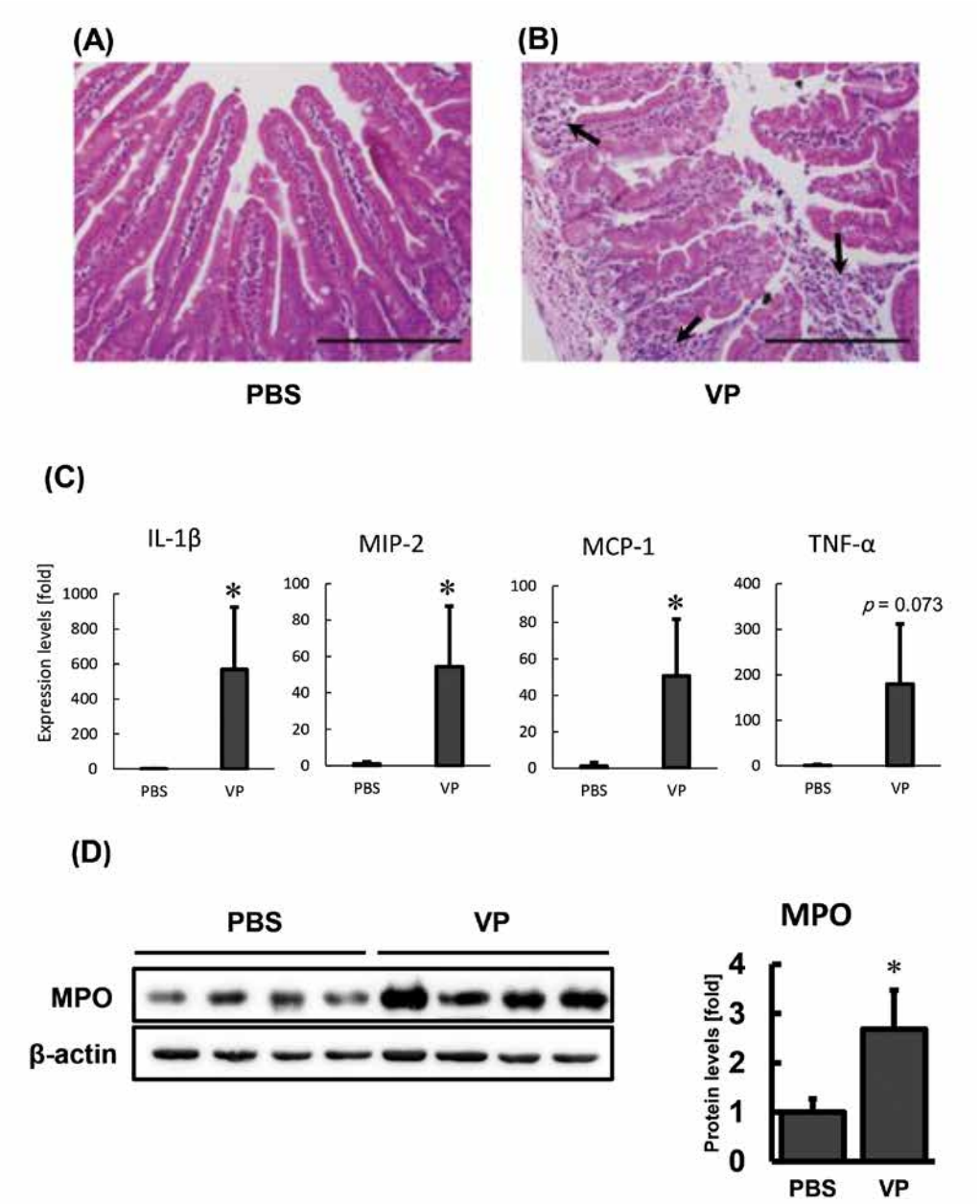

Fig 3. Confirmation of *V. parahaemolyticus*-induced neutrophil infiltration in mouse ileal tissue. (A, B) The intestinal tissues were infected with *V. parahaemolyticus* for 4 h or treated with PBS as a control samples under the loop model, and tissue were stained with HE and observed under a microscope. Scale bar = 50 μm. Arrows indicates neutrophil infiltration. The error bar indicates standard deviation. (C) Expression levels of mRNA in inflammatory cytokine were estimated by Real-time RT-PCR of mouse intestinal loops infected with *V. parahaemolyticus* for 4 h. Non-infected control (PBS) set as 1. The error bar indicates standard deviation. *$p < 0.05$ (PBS vs. VP ; Student's *t*-test). (D) MPO protein levels were estimated by western blot analysis of mouse intestinal loops infected with *V. parahaemolyticus* for 4 h. MPO was detected using specific Abs. β-actin was detected as a loading control. Relative band intensities were calculated. The error bar indicates standard deviation. *$p < 0.01$ (PBS vs. VP ; Student's *t*-test).

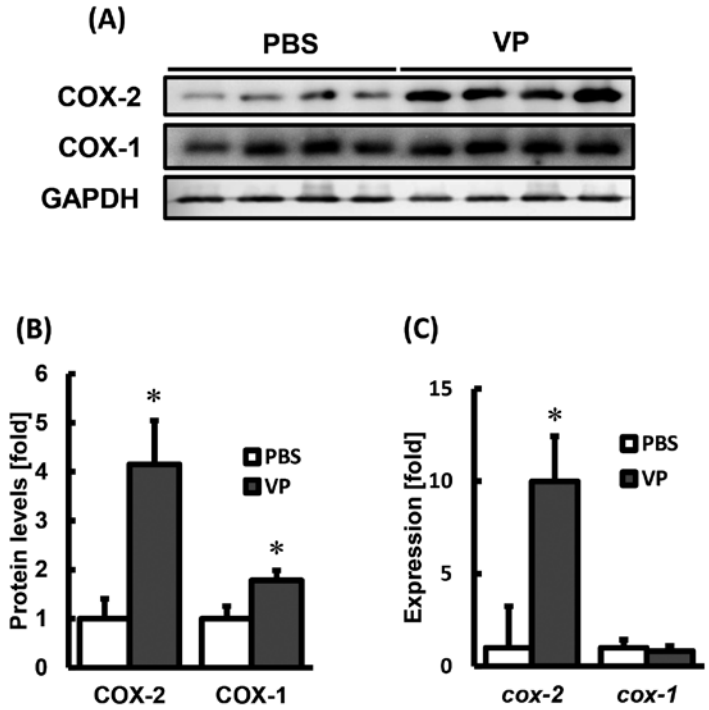

Fig 4. COX-2 expression levels in *V. parahaemolyticus*-infected mouse intestine. (A) COX-2 and COX-1 protein levels in mouse tissues were quantified by western blot analysis by using specific Abs. Glyceraldehyde 3-phosphate dehydrogenase was detected as a loading control. (B) Relative band intensities of COX-2 and COX-1. (C) COX-2 mRNA expression levels in mouse intestines were analyzed by real-time RT-PCR. The error bar indicates standard deviation. Data differing significantly from PBS are marked by * (Student's *t*-test). $*p < 0.01$

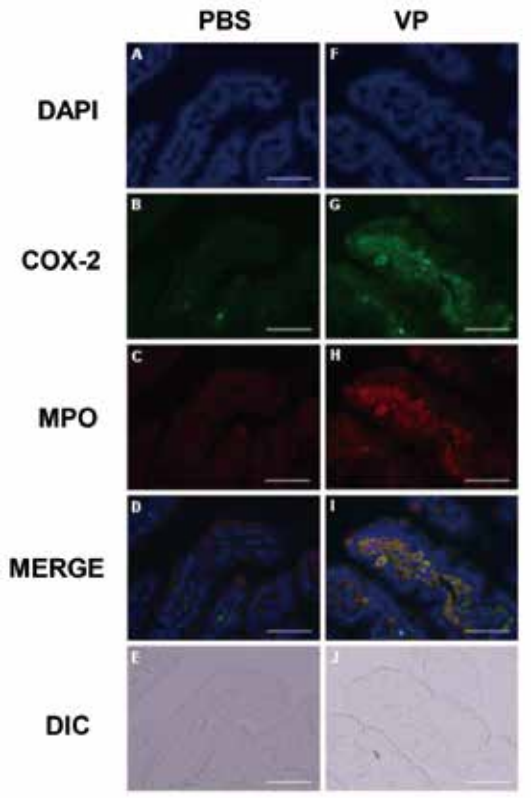

Fig 5. Distribution of COX-2 and MPO in the mouse intestine. Distribution of COX-2 and MPO were detected by immunofluorescence analysis with specific Abs. A, F : Nuclear localization. B, G : Distribution of COX-2. C, H : distribution of MPO. D, I : Colocalization of COX-2 and MPO. E, J : Differential interference contrast image. A-E : Non-infected tissue, F-J : Tissue infected with *V. parahaemolyticus* for 4 h. Scale bar = 50 μm.

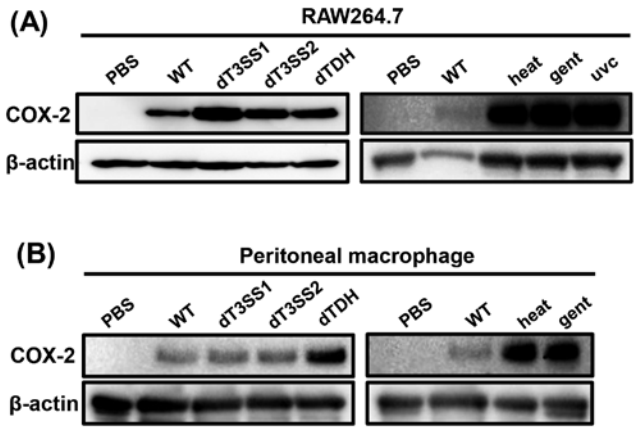

Fig S4. COX-2 expression levels in *V. parahaemolyticus*-infected RAW264.7 and peritoneal macrophage. COX-2 protein levels in *V. parahaemolyticus*-mutant strains or killed *V. parahaemolyticus* (95℃ 5 min heated, 100 μg/mL gentamicin treated, and 5 min exposed 280 nm: UVC) treated cells were estimated by western blot analysis in RAW264.7 (A) or mouse peritoneal macrophage (B) for 4 h treatment. Each cell lysates were normalized by protein contents. COX-2 was detected using specific Abs. β-actin was detected as a loading control.

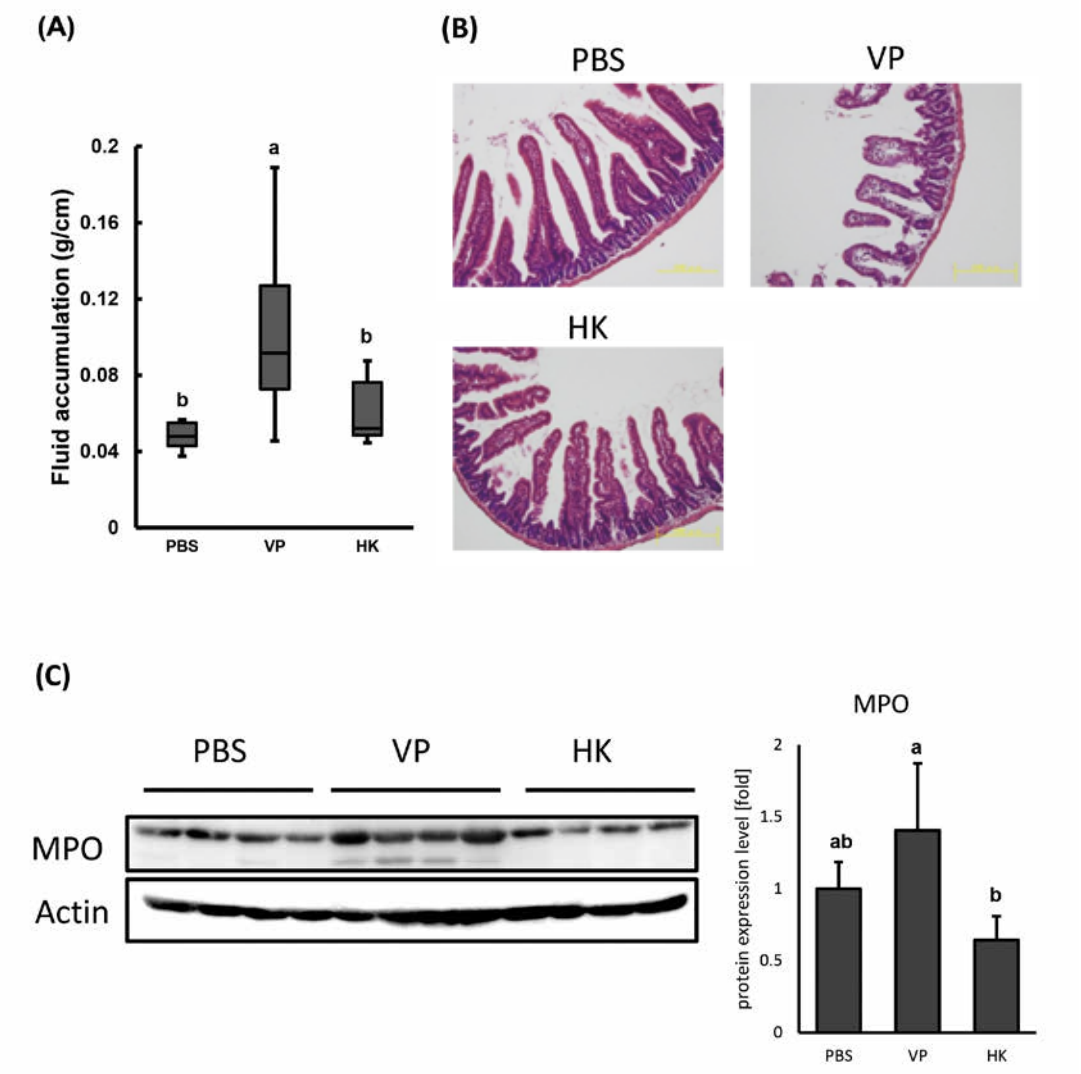

Fig S5. Infiltration of neutrophils in mouse intestine by Heat-killed-bacteria in vivo. (A) Bacterial suspension (VP ; wild type or HK ; heat-killed *V. parahaemolyticus*) or PBS was injected to the intestinal loops of mouse. After infection for 6 h, the loops were removed and fluid accumulation was calculated (n = 8 to 10). Box plot showing fluid accumulation, as determined with a mouse intestinal loop assay. Upper horizontal line of box, 75th percentile ; lower horizontal line of box, 25th percentile ; horizontal bar within box, median ; upper horizontal bar outside of box, maximum value ; lower horizontal bar outside of box, minimum value. Different letters of the alphabet indicate statistical difference ($p < 0.05$) from each other as determined by ANOVA with Tukey Kramer's test. (B) The mice were infected with *V. parahaemolyticus*, treated with Heat-killed-bacteria or PBS (control samples) for 6 h under the loop model, which tissues were stained with HE and observed under a microscope. Scale bar = 200 μm. (C) MPO protein levels were estimated by western blot analysis in each mouse. MPO was detected using specific Abs. β-actin was detected as a loading control. Relative band intensities were calculated. The error bar indicates standard deviation. Different letters of the alphabet indicate statistical difference ($p < 0.05$) from each other as determined by ANOVA with Tukey Kramer's test.

However, still effectors secretion rate or balance between T3SS1 and T3SS2 are not clear in infection site. On the other hand, the T3SS2 effecter protein VopV was identified as the main factor of F-actin-mediated diarrhea in rabbits, as confirmed with the loop test (14). Also, other T3SS2 effector proteins (i.e., VopL and VopC) modulate actin stress fibers (34-37). Still, a relationship between CFTR channel and actin fiber formation has been reported. CFTR activity is modulated by actin filament organization via a functional interaction that can be achieved independently via the cAMP-PKA-mediated regulatory pathway (38). It is also possible that *V. parahaemolyticus*-induced inflammation may promote T3SS2-induced modulation of actin filaments and facilitate CFTR-mediated *V. parahaemolyticus*-induced diarrhea.

There are many factors associated with the formation and function of ion channels in secretory diarrhea in the mouse loop model. However, the focus of the present study was limited to the effect of CFTR in *V. parahaemolyticus*-induced diarrhea. Unfortunately, it was not possible to completely reveal the underlying mechanisms. In our next study, we plan to investigate other diarrhea-associated channel factor, such as the calcium-activated chloride channels, which are activated in secretory diarrhea in *Vibrio cholerae* O1 El Tor variant induced diarrhea in mice (39), or GABA, which is a primary neurotransmitter in the central nervous system and also regulates the function of the gastrointestinal tract. These factors also participate in intestinal fluid secretion of the mouse (40). Hence, future investigations are warranted to further elucidate the mechanisms underlying fluid accumulation in response to *V. parahaemolyticus* infection.

CONCLUSION

This study reveals an important relationship between *V. parahaemolyticus*-induced diarrhea and inflammation in a mouse model. Our data suggested that *V. parahaemolyticus*-inducing infiltration and activation of neutrophils were closely associated with CFTR mediated fluid secretion. Our finding may serve to elucidate the mechanism of *V. parahaemolyticus*-induced diarrhea in detail.

CONFLICTS OF INTEREST

There is no actual or potential conflict of interest in this manuscript.

ACKNOWLEDGEMENTS

The metabolomics analysis platform was supported by the Support Center for The Special Mission Center for Metabolome Analysis, School of Medical Nutrition, Faculty of Medicine of Tokushima University. We are thankful to the Support Center for Advanced Medical Sciences, Institute of Biomedical Sciences, and Tokushima University Graduate School for providing research materials.

This work was supported by a grant-in-aid for scientific research from JSPS Kakenhi (grant number JP 25750043). The authors would like to thank enago (www.enago.jp/) for the English language review.

REFERENCES

1. Janda JM, Powers C, Bryant RG, Abbott SL : Current perspectives on the epidemiology and pathogenesis of clinically significant Vibrio spp. Clin Microbiol Rev 1 : 245-267, 1988
2. Alam NH, Chisti J, Kondo S, Sugiyama J, Bhuiyan NA, Mathan MM, Sack DA, Nair GB : Adaptive and inflammatory immune responses in patients infected with strains of Vibrio parahaemolyticus. J Infect Dis 187 : 1085-96, 2003
3. Park KS, Ono T, Rokuda M, Jang MH, Okada K, Iida T, Honda T : Functional characterization of two type III secretion systems of Vibrio parahaemolyticus. Infect Immun 72 : 6659-65, 2004
4. Ritchie JM, Rui H, Zhou X, Iida T, Kodoma T, Ito S, Davis BM, Bronson RT, Waldor MK : Inflammation and disintegration of intestinal villi in an experimental model for Vibrio parahaemolyticus-induced diarrhea. PLoS Pathog 8 : e1002593, 2012
5. Broberg CA, Calder TJ, Orth K : Vibrio parahaemolyticus cell biology and pathogenicity determinants. Microbes Infect 13 : 992-1001, 2011
6. Matsuda S, Kodama T, Okada N, Okayama K, Honda T, Iida T : Association of Vibrio parahaemolyticus thermostable direct hemolysin with lipid rafts is essential for cytotoxicity but not hemolytic activity. Infect Immun 78 : 603-10, 2010
7. Honda T, Ni Y, Miwatani T, Adachi T, Kim J : The thermostable direct hemolysin of Vibrio parahaemolyticus is a pore-forming toxin. Can J Microbiol 38:1175-80, 1992
8. Raghunath P : Roles of thermostable direct hemolysin (TDH) and TDH-related hemolysin (TRH) in Vibrio parahaemolyticus. Front Microbiol 22 : 805, 2015
9. Takahashi A, Sato Y, Shiomi Y, Cantarelli VV, Iida T, Lee M, Honda T : Mechanisms of chloride secretion induced by thermostable direct haemolysin of Vibrio parahaemolyticus in human colonic tissue and a human intestinal epithelial cell line. J Med Microbiol 49 : 801-810, 2000
10. Takahashi A, Iida T, Naim R, Naykaya Y, Honda T : Chloride secretion induced by thermostable direct haemolysin of Vibrio parahaemolyticus depends on colonic cell maturation. J Med Microbiol 50 : 870-878, 2001
11. Takahashi A, Kenjyo N, Imura K, Myonsun Y, Honda T : Cl(-) secretion in colonic epithelial cells induced by the vibrio parahaemolyticus hemolytic toxin related to thermostable direct hemolysin. Infect Immun 68 : 5435-8, 2000
12. Park KS, Ono T, Rokuda M, Jang MH, Iida T, Honda T : Cytotoxicity and enterotoxicity of the thermostable direct hemolysin-deletion mutants of Vibrio parahaemolyticus. Microbiol Immunol 48 : 313-8, 2004
13. Hiyoshi H, Kodama T, Iida T, Honda T : Contribution of Vibrio parahaemolyticus virulence factors to cytotoxicity, enterotoxicity, and lethality in mice. Infect Immun 78 : 1772-80, 2010
14. Hiyoshi H, Kodama T, Saito K, Gotoh K, Matsuda S, Akeda Y, Honda T, Iida T : VopV, an F-actin-binding type III secretion effector, is required for Vibrio parahaemolyticus-induced enterotoxicity. Cell Host Microbe 10 : 401-9, 2011
15. Matsuda S, Okada R, Tandhavanant S, Hiyoshi H, Gotoh K, Iida T, Kodama T : Export of a Vibrio parahaemolyticus toxin by the Sec and type III secretion machineries in tandem. Nat Microbiol 4 : 781-788, 2019
16. Hiyoshi H, Kodama T, Iida T, Honda T : Contribution of Vibrio parahaemolyticus virulence factors to cytotoxicity, enterotoxicity, and lethality in mice. Infect Immun 78 : 1772-80, 2010
17. Piñeyro P, Zhou X, Orfe LH, Friel PJ, Lahmers K, Call DR : Development of two animal models to study the function of Vibrio parahaemolyticus type III secretion systems.

Infect Immun 78 : 4551-9, 2010
18. Makino K, Oshima K, Kurokawa K, Yokoyama K, Uda T, Tagomori K, Iijima Y, Najima M, Nakano M, Yamashita A, Kubota Y, Kimura S, Yasunaga T, Honda T, Shinagawa H, Hattori M, Iida T : Genome sequence of Vibrio parahaemolyticus : a pathogenic mechanism distinct from that of V cholerae. Lancet 361 : 743-9, 2003
19. Bhattacharjee RN, Park KS, Kumagai Y, Okada K, Yamamoto M, Uematsu S, Matsui K, Kumar H, Kawai T, Iida T, Honda T, Takeuchi O, Akira S : VP1686, a Vibrio type III secretion protein, induces toll-like receptor-independent apoptosis in macrophage through NF-kappaB inhibition. J Biol Chem 281 : 36897-904, 2006
20. Burdette DL, Yarbrough ML, Orvedahl A, Gilpin CJ, Orth K : Vibrio parahaemolyticus orchestrates a multifaceted host cell infection by induction of autophagy, cell rounding, and then cell lysis. Proc Natl Acad Sci U S A 105 : 12497-502, 2008
21. Shimohata T, Nakano M, Lian X, Shigeyama T, Iba H, Hamamoto A, Yoshida M, Harada N, Yamamoto H, Yamato M, Mawatari K, Tamaki T, Nakaya Y, Takahashi A : Vibrio parahaemolyticus infection induces modulation of IL-8 secretion through dual pathway via VP1680 in Caco-2 cells. J Infect Dis 203 : 537-44, 2011
22. Zhou X, Konkel ME, Call DR : Regulation of type III secretion system 1 gene expression in Vibrio parahaemolyticus is dependent on interactions between ExsA, ExsC, and ExsD. Virulence 1 : 260-72, 2010
23. Low-Beer TS, Read AE : Diarrhoea : mechanisms and treatment. Gut 12 : 1021-36, 1971
24. Golin-Bisello F, Bradbury N, Ameen N : STa and cGMP stimulate CFTR translocation to the surface of villus enterocytes in rat jejunum and is regulated by protein kinase G. Am J Physiol Cell Physiol 289 : C708-16, 2005
25. Fujii Y, Tsurumi K, Sato M, Takahashi E, Okamoto K : Fluid secretion caused by aerolysin-like hemolysin of Aeromonas sobria in the intestines is due to stimulation of production of prostaglandin E2 via cyclooxygenase 2 by intestinal cells. Infect Immun 76 : 1076-82, 2008
26. Whitmarsh AJ, Davis RJ : Transcription factor AP-1 regulation by mitogen-activated protein kinase signal transduction pathways. J Mol Med (Berl) 74 : 589-607, 1996
27. Ma T, Thiagarajah JR, Yang H, Sonawane ND, Folli C, Galietta LJ, Verkman AS : Thiazolidinone CFTR inhibitor identified by high-throughput screening blocks cholera toxin-induced intestinal fluid secretion. J Clin Invest 110 : 1651-8, 2002
28. Thiagarajah JR, Broadbent T, Hsieh E, Verkman AS : Prevention of toxin-induced intestinal ion and fluid secretion by a small-molecule CFTR inhibitor. Gastroenterology 126 : 511-9, 2004
29. Schultz BD, Singh AK, Devor DC, Bridges RJ : Pharmacology of CFTR chloride channel activity. Physiol Rev 79 : S109-44, 1999
30. Smith G, Warhurst G, Lees M, Turnberg L : Evidence that PGE2 stimulates intestinal epithelial cell adenylate cyclase by a receptor-mediated mechanism. Dig Dis Sci 32 : 71-5, 1987
31. Matlawska-Wasowska K, Finn R, Mustel A, O'Byrne CP, Baird AW, Coffey ET, Boyd A : The Vibrio parahaemolyticus Type III Secretion Systems manipulate host cell MAPK for critical steps in pathogenesis. BMC Microbiol 10 : 329, 2010
32. Zhou X, Gewurz BE, Ritchie JM, Takasaki K, Greenfeld H, Kieff E, Davis BM, Waldor MK : A Vibrio parahaemolyticus T3SS effector mediates pathogenesis by independently enabling intestinal colonization and inhibiting TAK1 activation. Cell Rep 3 : 1690-702, 2013
33. Trosky JE, Mukherjee S, Burdette DL, Roberts M, McCarter L, Siegel RM, Orth K : Inhibition of MAPK signaling pathways by VopA from Vibrio parahaemolyticus. J Biol Chem 279 : 51953-7, 2004
34. Zahm JA, Padrick SB, Chen Z, Pak CW, Yunus AA, Henry L, Tomchick DR, Chen Z, Rosen MK : The bacterial effector VopL organizes actin into filament-like structures. Cell 155 : 423-34, 2013
35. Yu B, Cheng HC, Brautigam CA, Tomchick DR, Rosen MK : Mechanism of actin filament nucleation by the bacterial effector VopL. Nat Struct Mol Biol 18 : 1068-74, 2011
36. Liverman AD, Cheng HC, Trosky JE, Leung DW, Yarbrough ML, Burdette DL, Rosen MK, Orth K : Arp2/3-independent assembly of actin by Vibrio type III effector VopL. Proc Natl Acad Sci U S A 104 : 17117-22, 2007
37. Okada R, Zhou X, Hiyoshi H, Matsuda S, Chen X, Akeda Y, Kashimoto T, Davis BM, Iida T, Waldor MK, Kodama T : The Vibrio parahaemolyticus effector VopC mediates Cdc42-dependent invasion of cultured cells but is not required for pathogenicity in an animal model of infection. Cell Microbiol 16 : 938-47, 2014
38. Cantiello HF : Role of the actin cytoskeleton in the regulation of the cystic fibrosis transmembrane conductance regulator. Exp Physiol 81 : 505-14, 1996
39. Satitsri S, Pongkorpsakol P, Srimanote P, Chatsudthipong V, Muanprasat C : Pathophysiological mechanisms of diarrhea caused by the Vibrio cholerae O1 El Tor variant : an in vivo study in mice. Virulence 7 : 789-805, 2016
40. Li Y, Xiang YY, Lu WY, Liu C, Li J : A novel role of intestine epithelial GABAergic signaling in regulating intestinal fluid secretion. Am J Physiol Gastrointest Liver Physiol 303 : G453-60, 2012